SrFe$_{12}$O$_{19}$ based ceramics with ultra-low dielectric loss in the millimetre-wave band

Chuying Yu[1,2], Yang Zeng[3,4], Bin Yang[5,a)], Richard Wylde[6], Robert Donnan[3], Jiyue Wu[1], Jie Xu[7], Feng Gao[7], Isaac Abrahams[8], Mike Reece[1], Haixue Yan[1]

[1] School of Engineering and Materials Science, Queen Mary University of London, London, E1 4NS, UK

[2] College of Materials Science and Engineering, Hunan University, Changsha, 410082, People's Republic of China

[3] School of Electronic Engineering and Computer Science, Queen Mary University of London, London, E1 4NS, UK

[4] Academy of Ocean Science and Engineering, National University of Defence Technology, Changsha, 410073, People's Republic of China

[5] Department of Electronic and Electrical Engineering, University of Chester, Chester, CH2 4NU, UK

[6] Thomas Keating Ltd, Billingshurst, West Sussex, RH14 9SH, UK.

[7] Department of Materials Science and Engineering, Northwestern Polytechnical University, Xi'an 710072, People's Republic of China

[8] School of Biological and Chemical Sciences, Queen Mary University of London, London, E1 4NS, UK

a) Electronic mail: b.yang@chester.ac.uk

Abstract

Non-reciprocal devices such as isolators and circulators, based mainly on ferromagnetic materials, require extremely low dielectric loss in order for strict power-link budgets to be met for millimetre (mm)-wave and terahertz (THz) systems. The dielectric loss of commercial SrFe$_{12}$O$_{19}$ hexaferrite was significantly reduced to below 0.002 in the 75 - 170 GHz band by thermal annealing. While the overall concentration of Fe^{2+} and oxygen vacancy defects is relatively low in

the solid, their concentration at the surface is significantly higher, allowing for a surface sensitive technique such as XPS to monitor the Fe^{3+}/Fe^{2+} redox reaction. Oxidation of Fe^{2+} and a decrease in oxygen vacancies is found at the surface on annealing, which is reflected in the bulk sample by a small change in unit cell volume. The significant decrease in dielectric loss property can be attributed to the decreased concentration of charged defects such as Fe^{2+} and oxygen vacancies through annealing process, which demonstrated that thermal annealing could be effective in improving the dielectric performance of ferromagnetic materials for various applications.

Introduction

High performance Faraday devices (*i.e.* those having low insertion loss and strong gyrotropic action), are in high demand for future mm and sub-mm wave radiometers to be deployed for astronomy and cosmology. [1-3] Commercial M-type hexaferrite $SrFe_{12}O_{19}$-based ceramics are the preferred choice in electromagnetic mm-wave non-reciprocal devices, such as isolators and circulators, and for other types of derivative components such as filters and resonators. [4-7] However, the limited availability of ultra-low dielectric loss hexaferrites is inhibiting the development of mm-wave and THz technologies. This is due to the fact that the Fe^{3+} ions are easily reduced to Fe^{2+} during sintering. The consequence is a dramatic deterioration in the requisite dielectric properties via an electron-hopping mechanism between Fe^{3+} and Fe^{2+} ions in octahedral sites. [8,9]

The desired mm-wave dielectric properties of ferrites can be engineered by cation-substitution. Partial substitution of Sr^{2+} with trivalent ions such as Al^{3+}, Cr^{3+} and La^{3+} has been

reported to be associated with a valence change of Fe^{3+} to Fe^{2+} at $2a$- or $4f_2$- sites, which increases the dielectric permittivity, but simultaneously increases the dielectric loss. [10-12] Various synthesis routes and processing conditions have been investigated in order to control the microstructure and ultimately to modify magnetic and dielectric properties. [13,14] Chief among them, thermal annealing is highlighted here as being instrumental in manipulating microstructure and chemical composition. However, it has been rarely used to study the relationship between dielectric properties and point defects in strontium ferrite. [15]

In this letter, the effect of thermal annealing on the dielectric properties of commercial $SrFe_{12}O_{19}$-based ceramics is presented. A significant 66% decrease in dielectric loss was achieved by thermal annealing, which is attributed to the oxidation of Fe^{2+} and decrease in oxygen vacancy concentration.

Experimental

Commercial strontium hexaferrite ($SrFe_{12}O_{19}$)-based samples were obtained from the TDK Corporation, Japan. There were two groups of samples: as-received samples from TDK Ltd. and those annealed by Thomas Keating Ltd. The sample is 10 cm×10 cm square size and the thickness is 2.018(±0.002) mm. The structures of the as-received and annealed samples were analysed by X-ray powder diffraction (XRD, X'pert Pro, PANalytical, Almelo, Netherlands) using Ni filtered Cu-Kα (1.5418 Å) radiation, over the 2θ range 5° to 120°, in steps of 0.0167°, with an effective scan-time of 200 s per step for the X'Celerator detector. Data analysis was carried out using the Rietveld method with the General Structure Analysis System (GSAS) software. [16] The initial

structural model was based on that of Zi *et al*. in space group $P6_3/mmc$. [17] The microstructure of

the specimens was examined using a scanning electron microscope (SEM, FEI, Inspect F, Hillsboro,

OR). Elemental analysis was carried out by Energy-Dispersive X-ray spectroscopy (EDX, Oxford

instruments). The electron energy states of elements in the samples were determined using X-

ray photoelectron spectroscopy (XPS, ESCALAB MK II, VG Scientific). XPS peak-fitting was

processed using Origin 9.0 software, with all peaks being fitted based on the Lorentzian-Gaussian

model. [18] The complex dielectric response of the samples was measured using a vector network

analyser (VNA)-driven quasi-optical transmissometer operating over contiguous waveguide

bands covering 75 to 170 GHz. [19]

Results and discussion

Fig. 1 shows XRD patterns of the studied samples, with the fitted diffraction profiles given

in the supporting information as Fig. S1 and the corresponding crystal and refinement

parameters presented in Table S1. The results confirmed that the samples were both hexagonal-

structured strontium ferrite with (00*l*) preferred orientation. The patterns agree well with the

standard pattern (PDF No. 33-1340), although it is noted that the unit cell volume is smaller than

that of the standard pattern (691.38 Å^3). Indeed, the unit cell volume varies significantly between

reports in the literature with Muller and Collomb [20], reporting a value of 689.85 Å^3, Zi *et al*. [17] a

value of 688.71 Å^3 and Luo *et al*. [21] a value of 690.68 Å. The difference in these values reflects

differing degrees of Fe^{3+} reduction, with a significant difference in ionic radius between Fe^{3+} and

Fe^{2+} (r = 0.645 Å and 0.780 Å, respectively, for the ions in high-spin octahedral geometries [22]). In

the present case, the lower unit cell volume might suggest a higher degree of oxidation than seen

in the previous reports. There is a very small reduction in unit volume on annealing, consistent

4

with a degree of oxidation, but no other significant structural changes were observed between the as-received and the annealed samples. The reduction of Fe^{3+} to Fe^{2+} leads to formation of oxygen vacancies (eq. 1)[23].
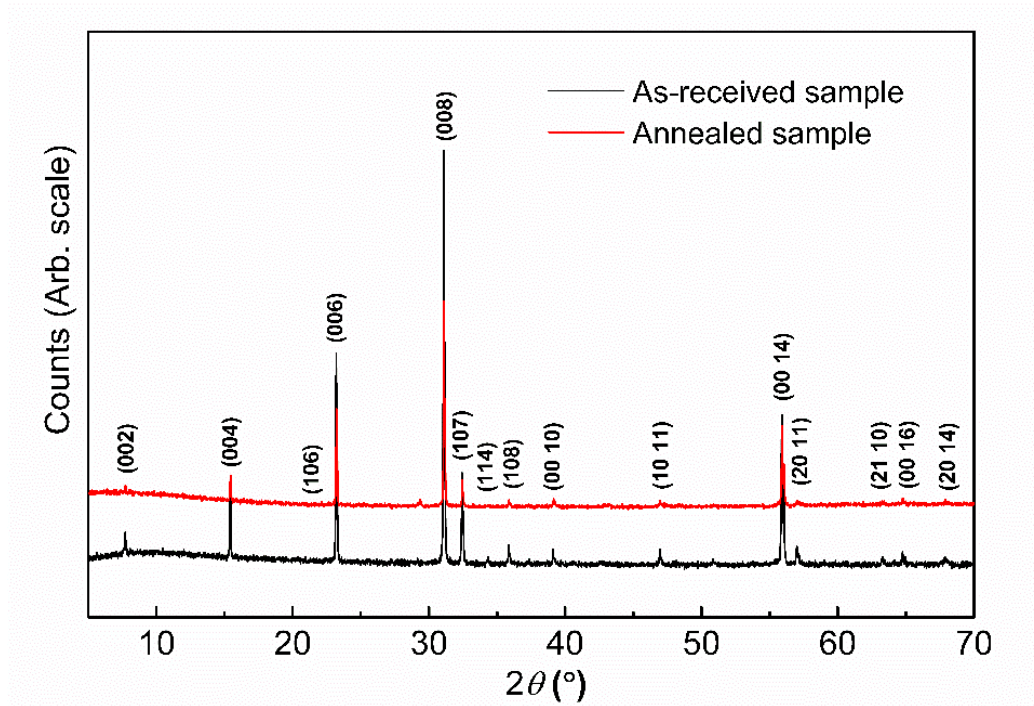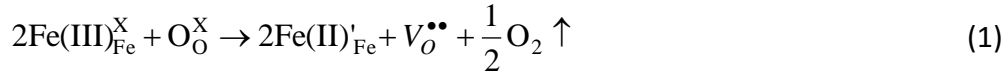
$$2Fe(III)_{Fe}^{X} + O_{O}^{X} \rightarrow 2Fe(II)_{Fe}' + V_{O}^{\bullet\bullet} + \frac{1}{2}O_{2} \uparrow \qquad (1)$$

Fig. 1. XRD patterns of as-received and annealed samples of $SrFe_{12}O_{19}$.

SEM micrographs of the as-received and annealed samples with the corresponding EDX spectra are shown in Fig. 2. Uniformly aligned columnar-shaped grains of homogenous size were observed for both the as-received (Fig. 2a) and annealed (Fig. 2b) samples, consistent with the preferred orientation observed in the XRD profiles. The EDX analysis of as-received (Fig. 2c) and annealed (Fig. 2d) samples identified minor amounts of Al and Ca, as well as the expected Sr and

Fe. Low levels of Al_2O_3 and $CaCO_3$ are typically added in production to limit grain growth and improve the magnetic and dielectric properties of strontium hexaferrite. [11,13]
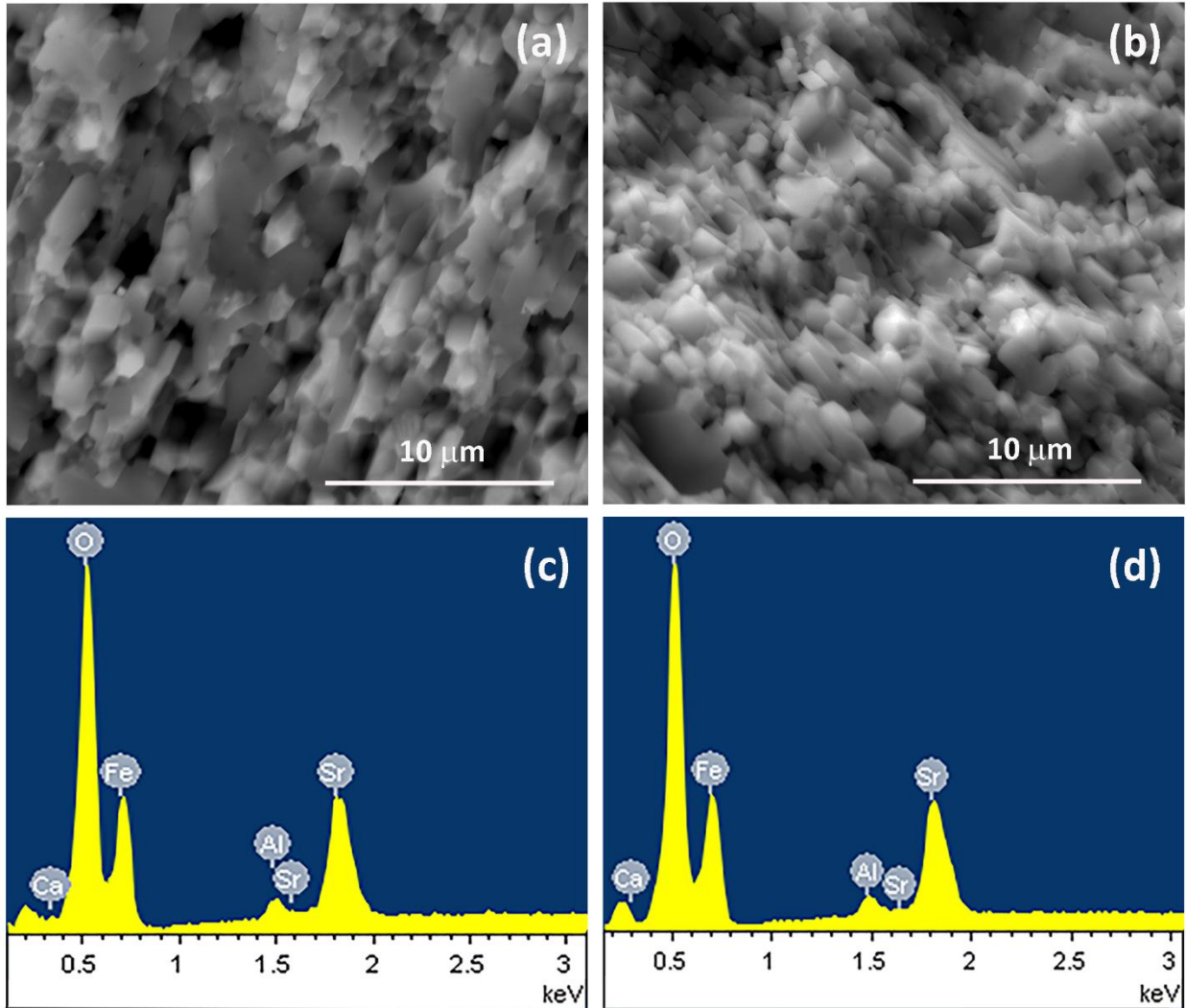

Fig. 2. SEM micrographs of (a) as-received and (b) annealed samples of $SrFe_{12}O_{19}$; EDX spectra of (c) as-received and (d) annealed samples of $SrFe_{12}O_{19}$.

XPS spectra covering the Fe $2p$ peaks for the as-received and annealed samples are presented in Figs. 3a and 3b, respectively. Spin-orbit coupling splits the Fe $2p$ peak into a doublet,

corresponding to Fe $2p_{3/2}$ and Fe $2p_{1/2}$ [24]. The obtained binding energies are summarised in Table 1. Interestingly, curve fitting confirmed that both samples contained iron in the 0, 2+ and 3+ oxidation states. Integration of the Fe $2p_{3/2}$ peaks reveals the percentage distribution of these oxidation states as 9% Fe^0, 59% Fe^{2+} and 38% Fe^{3+} in the as-received sample, which changes to 6% Fe^0, 46% Fe^{2+} and 48% Fe^{3+} for the annealed sample. The presence of Fe^0 and Fe^{2+} in the XPS spectra indicates significant reduction of Fe^{3+}. XPS is a particularly surface sensitive technique. The present results show much higher concentrations of reduced iron species than are expected in the bulk. Indeed, the X-ray powder diffraction data, which are more representative of the bulk ceramic, confirm a relatively low level of reduction in these samples. The advantage of using XPS, in this instance, is that the levels of reduced species are greatly enhanced at the ceramic surface, allowing for the effects of annealing to be more readily visualized. On annealing, there is an obvious decrease in intensity of the lower oxidation states and increase in that of Fe^{3+}, confirming a degree of oxidation. This is consistent with the small decrease in unit cell volume seen in the XRD analysis.
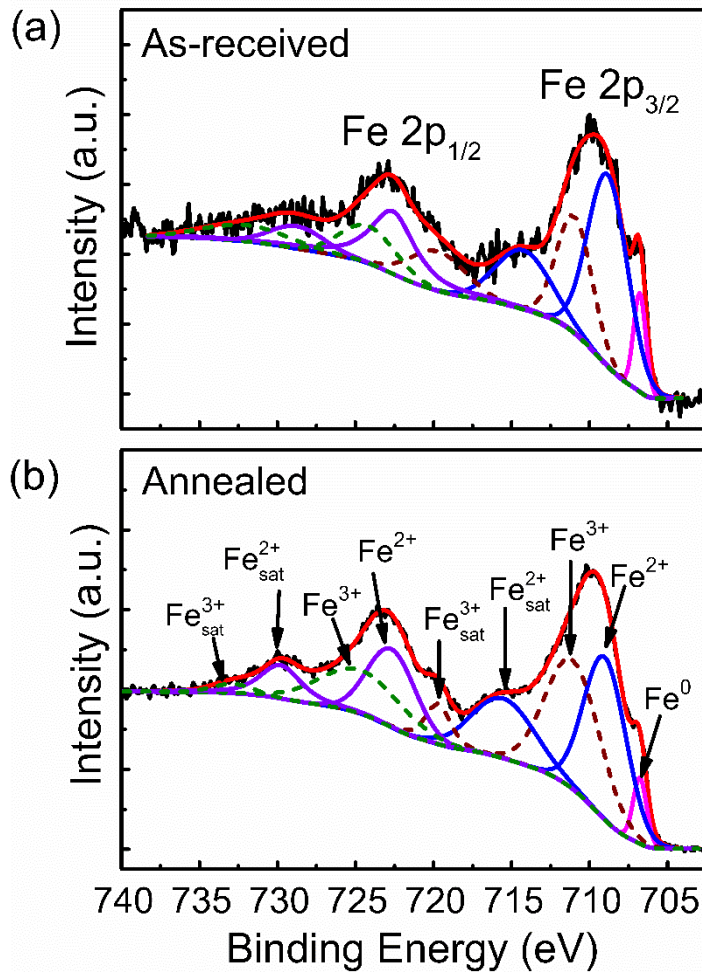
Fig. 3. XPS spectra showing Fe 2*p* peaks for (a) as-received and (b) annealed samples of $SrFe_{12}O_{19}$ (*sat* denotes for *satellite*).

XPS spectra for the O 1*s* peaks for both the as-received and annealed samples are presented in Fig. 4. The O 1*s* spectra were modelled using a convolution of three peaks. For the as-received sample (Fig. 4a), the peak at 530.1 eV represents oxygen on its intrinsic site; the peak at 531.2 eV is related to the oxygen in the reduced region; and the peak at 533.0 eV is chemisorbed oxygen on the surface of the sample. [25] For the annealed samples (Fig. 4b), these peak position shift slightly to 530.2 eV, 531.5 eV and 533.2 eV, respectively. Integration of the

intrinsic and reduced region peaks reveals a ratio of 62% to 38%, respectively, for the as-received sample. This ratio increases to 67:33, post-annealing, consistent with a decrease in the number of oxide ion vacancies on annealing.
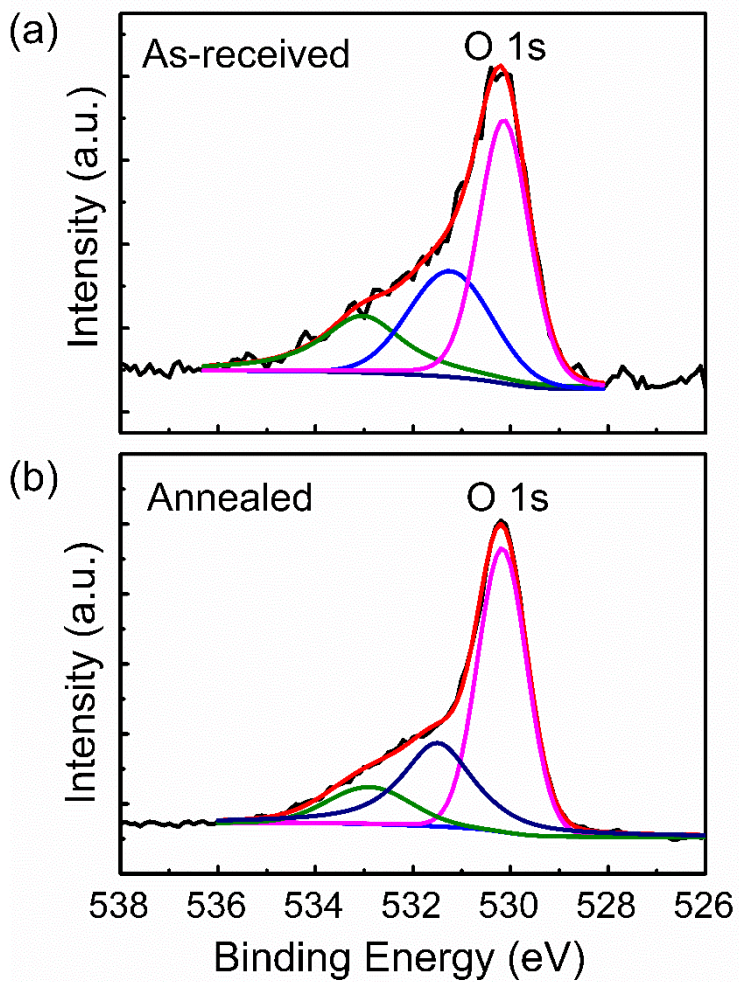

Fig. 4 XPS spectra showing O 1s peaks for (a) as-received and (b) annealed samples of SrFe$_{12}$O$_{19}$.

Table 1 Fe 2p binding energies obtained from XPS spectra for as-received and annealed samples of SrFe$_{12}$O$_{19}$.

sample	Fe $^{2+}$ peak positions (eV)				Fe $^{3+}$ peak positions (eV)			
	satellite	Fe 2$p_{1/2}$	Satellite	Fe 2$p_{3/2}$	satellite	Fe 2$p_{1/2}$	satellite	Fe 2$p_{3/2}$
As-received	728.7	722.6	714.2	708.8	732	724.2	719.7	711.0
Annealed	729.8	722.7	715.5	709.0	732.8	724.7	719.7	711.1

The mm-wave transmission response of the sample was measured using a quasi-optical transmission system driven by a VNA. The detailed experimental and theoretical analyses are explained in the supporting information. The annealing treatment has no significant effect upon magnetic resonance and strength, as discussed in the supporting information. Thus, the nonlinear-curve fitting of the measured data against the theoretical model focusses on the effects of annealing on the dielectric properties. The calculated co-polar ($/\!/$) and cross-polar ($\perp$) S$_{21}$ scattering parameters based on the model and the experimental results are presented in Fig. 5 for both as-received and annealed samples. The frequency bands of analysis span 75 to 170 GHz, significantly away from the known magnetic resonance near 40 GHz. Dielectric loss is seen to be significantly reduced on annealing.
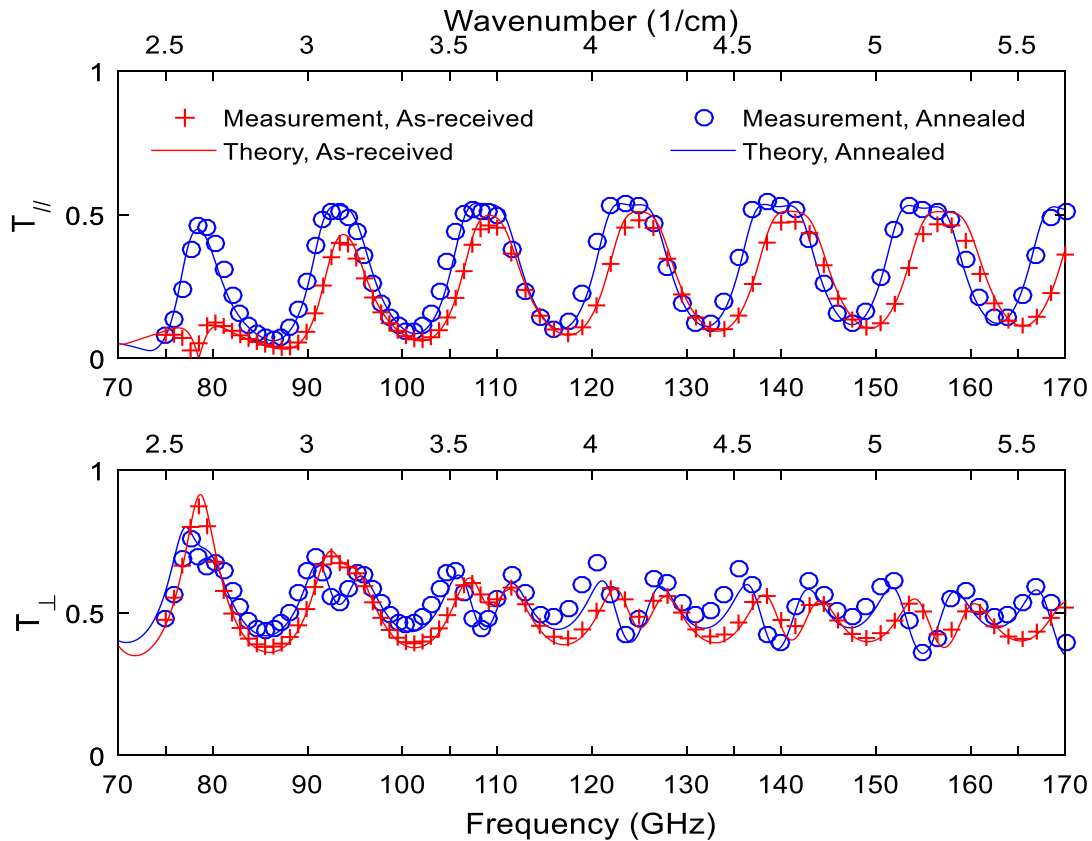
Fig. 5. Co- and cross-polar transmission data of as-received (red curves) and annealed (blue curves) samples of $SrFe_{12}O_{19}$. Solid lines denote theoretical calculations with respect to a physical model and discrete points are measured data.

Fig. 6 shows the frequency-dependent dielectric response of samples in the mm-wave band. Permittivity values of *ca.* 20.09 and 20.21 were obtained for the as-received and annealed samples, respectively. The dielectric loss of the annealed samples (below 0.002) is reduced by two thirds with respect to that of the as-received samples (which are above 0.006). The improvement in dielectric loss as a function of frequency is dispersive but slightly better improvement can be observed at higher frequency. The major contributor to dielectric loss in $SrFe_{12}O_{19}$–based ceramics is charged defects (Fe^{2+} and oxygen vacancies, eq. 1). [11,12,26] Electron hopping can occur between Fe^{3+} and Fe^{2+} cations. [26] Our results show that the number of charged defects is dramatically decreased by annealing (Fig. 3 and 4), which results in a significant

decrease in dielectric loss. Thus, the annealing process is clearly important in obtaining improved dielectric properties.
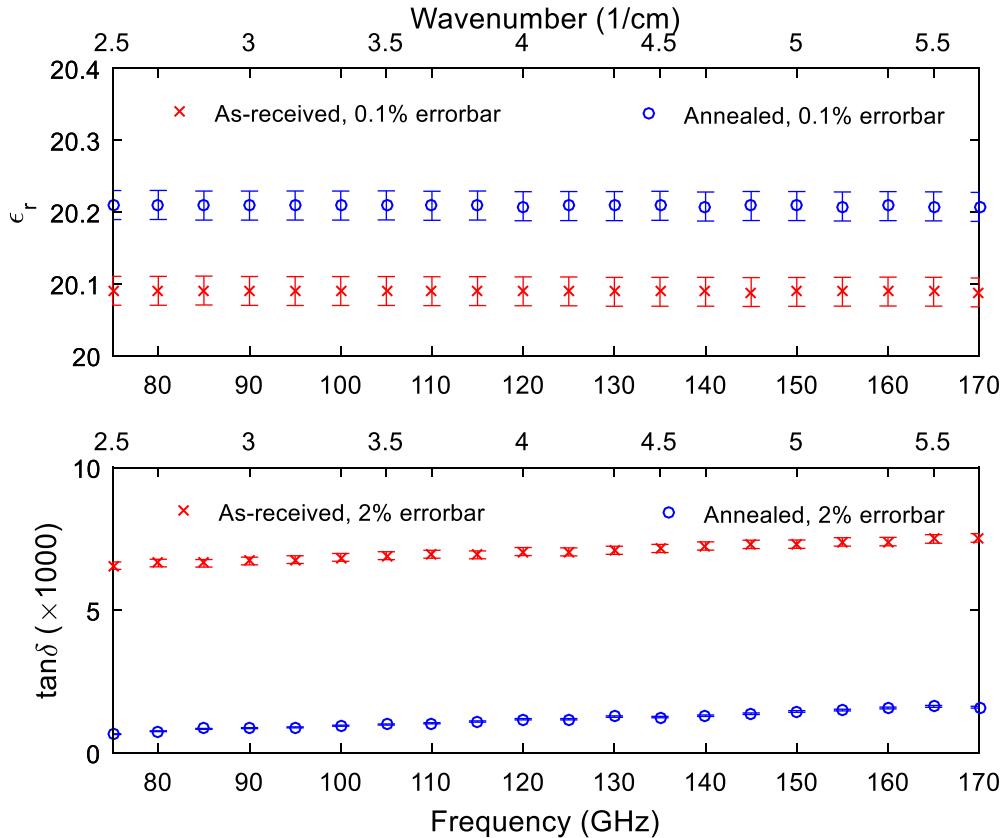

Fig. 6. Dispersive permittivity and dielectric loss performance of as-received and annealed samples of SrFe$_{12}$O$_{19}$, over the spectral domain spanning 75 – 110 GHz.

Conclusions

Annealing commercial hexaferrite SrFe$_{12}$O$_{19}$-based ceramics significantly reduces their dielectric loss in the mm-wave band. Annealing allows for the oxidation of Fe^{2+}, with an associated reduction in oxygen vacancies. While the concentration of these defects is relatively low in the main bulk of the solid, they can have a significant influence on the dielectric performance. There

is a much higher concentration of these defects at the ceramic surface, allowing for the redox

reaction to be probed using a surface sensitive technique, such as XPS. There is a clear decrease

in the vacancy concentration in these surface areas on annealing, which is reflected in a small

change in the unit cell volume, confirming that the oxidation occurs throughout the sample. The

improvement of dielectric loss performance of ceramic hexaferrites on annealing, will help

inform the manufacture of high-performance, mm and sub-mm wave non-reciprocal

components, such as non-reciprocal isolators and circulators. These are integral to radiometers

for planed Earth-observation and cosmological missions by the major national space agencies.

Supplementary Material

See supplementary material for the fitted XRD diffraction profiles, crystals and refinement

parameters, and also the method of mm-wave spectroscopy measurement.

Acknowledgements

References

[1] Francisca Maria Martins Pereira, CAR Junior, Manoel Roberval Pimentel Santos, Ricardo Sávio Teixeira Moretz Sohn, Francisco Nivaldo Aguiar Freire, Jose Marcos Sasaki, JAC De Paiva, and Antonio Sergio Bezerra Sombra, J. Mater. Sci. - Mater. El. **19** (7), 627 (2008).

[2] Tatsuya Nakamura, J. Appl. Phys. **88** (1), 348 (2000).

[3] Mitsuo Sugimoto, J. Am. Ceram. Soc. **82** (2), 269 (1999).

[4] H Khanduri, M Chandra Dimri, H Kooskora, I Heinmaa, G Viola, H Ning, MJ Reece, J Krustok, and R Stern, J. Appl. Phys. **112** (7), 073903 (2012).

[5] Robert C Pullar, Prog. Mater Sci. **57** (7), 1191 (2012).

[6] Mostafa Shalaby, Marco Peccianti, Yavuz Ozturk, and Roberto Morandotti, Nat. Commun. **4**, 1558 (2013).

[7] Kyunghan Ahn, Byungki Ryu, Dmitry Korolev, and Young Jae Kang, Appl. Phys. Lett. **103** (24), 242417 (2013).

8   N Rezlescu and E Rezlescu, Solid State Commun. **14** (1), 69 (1974).
9   Muhammad Javed Iqbal and Muhammad Naeem Ashiq, Chem. Eng. J. **136** (2), 383 (2008).
10   Xiansong Liu, Wei Zhong, Sen Yang, Zhi Yu, Benxi Gu, and Youwei Du, J. Magn. Magn. Mater. **238** (2), 207 (2002).
11   A Singh, SB Narang, K Singh, P Sharma, and OP Pandey, Eur Phys J-Appl Phys **33** (03), 189 (2006).
12   S Bindra Narang, Anterpreet Singh, and Kulwant Singh, J. Ceram. Process Res. **8** (5), 347 (2007).
13   FMM Pereira and ASB Sombra, in *Solid State Phenomena* (Trans Tech Publ, 2013), Vol. 202, pp. 1.
14   FJ Berry, JF Marco, CB Ponton, and KR Whittle, J. Mater. Sci. Lett. **20** (5), 431 (2001).
15   C Doroftei, E Rezlescu, P Dorin Popa, and N Rezlescu, Cryst. Res. Technol. **41** (11), 1112 (2006).
16   AC Larson and RB Von Dreele, Los Alamos National Laboratory, Los Alamos, NM (1986).
17   ZF Zi, YP Sun, XB Zhu, ZR Yang, and WH Song, J. Magn. Magn. Mater. **320** (21), 2746 (2008).
18   R Hesse, P Streubel, and R Szargan, Surf. Interface Anal. **39** (5), 381 (2007).
19   Bin Yang, Richard J Wylde, Derek H Martin, Philippe Goy, Robert S Donnan, and Sylvain Caroopen, IEEE Trans. Microwave Theory Tech. **58** (12), 3587 (2010).
20   J Muller and A Collomb, J. Magn. Magn. Mater. **103** (1-2), 194 (1992).
21   H Luo, BK Rai, SR Mishra, VV Nguyen, and JP Liu, J. Magn. Magn. Mater. **324** (17), 2602 (2012).
22   RD t Shannon, Acta Crystallographica Section A: Crystal Physics, Diffraction, Theoretical and General Crystallography **32** (5), 751 (1976).
23   Benfang Yu, Meiya Li, Jun Liu, Dongyun Guo, Ling Pei, and Xingzhong Zhao, J. Phys. D: Appl. Phys. **41** (6), 065003 (2008).
24   Toru Yamashita and Peter Hayes, Appl. Surf. Sci. **254** (8), 2441 (2008).
25   Chuying Yu, Yang Zeng, Bin Yang, Robert Donnan, Jinbao Huang, Zhaoxian Xiong, Amit Mahajan, Baogui Shi, Haitao Ye, and Russell Binions, Sci. Rep. **7** (2017).
26   K Iwauchi and Y Ikeda, physica status solidi (a) **93** (1), 309 (1986).